Available online at www.sciencedirect.com
ScienceDirect
Journal of Nuclear Materials 363–365 (2007) 1160–1167
journal of nuclear materials
www.elsevier.com/locate/jnucmat

Disruption mitigation on Alcator C-Mod using high-pressure gas injection: Experiments and modeling toward ITER

D.G. Whyte [a,*], R. Granetz [b], M. Bakhtiari [a], V. Izzo [b], T. Jernigan [c], J. Terry [b], M. Reinke [b], B. Lipschultz [b]

[a] University of Wisconsin – Madison, Madison, WI 53706, USA
[b] Plasma Science and Fusion Center, M.I.T., Cambridge, MA, USA
[c] Oak Ridge National Laboratory, Oak Ridge, TN, USA

Abstract

High-pressure gas-jet injection disruption mitigation is investigated on Alcator C-Mod. The experimental results are encouraging for ITER. Gas-jets delivers reliable and substantial disruption mitigation of thermal loads and halo currents at the ITER field and pressure. The gas injection is compatible with a metallic wall. The gas-jets provide sufficient radiative energy dissipation on a timescale even faster than required for ITER. Runaway electrons are suppressed, however a better understanding of this suppression is still required for ITER. Present 0-D calculations of the gas delivery and global plasma response match important experimental data such as overall quench time and the current quench L/R time. Frictional dissipation may be important for gas delivery down the long tubes that will probably be required for ITER. However deep gas and/or impurity penetration is not required for mitigation, relieving technical requirements for the gas pressure in ITER. Initial studies with the non-ideal MHD simulation NIMROD show that radiation-induced MHD plays a critical role in thermal quench particle and energy dynamics. The application of a newly available version of NIMROD, with more complete atomic physics, shows promise in matching the experimental trends and could be an invaluable tool for increasing our confidence in designing efficient disruption mitigation for ITER.

1. Introduction and motivation for Alcator C-Mod disruption studies

The rapid and uncontrolled loss of thermal (W_{th}) and poloidal magnetic energy (W_{pol}) associated with disruptions will likely cause unacceptable damage to in-vessel components of the burning plasma experiment, ITER [1] or envisioned tokamak reactors (e.g. [2]). In the simplest sense the disruption issue is more severe for these future devices because they have larger major radii, R, and plasma pressure ($p \sim W_{th}/R^3$) than present tokamaks. The decreasing surface to volume ratio of these plasmas ($\sim 1/R$) results in a much larger *areal* energy density $\varepsilon \sim (W_{th} + W_{pol})/R^2$, and hence greater potential to damage surrounding materials if the energy is lost in the timescales associated with disruptions ($\sim$1–10 ms).

* Corresponding author.
E-mail address: whyte@psfc.mit.edu (D.G. Whyte).

0022-3115/$ - see front matter © 2007 Elsevier B.V. All rights reserved.
doi:10.1016/j.jnucmat.2007.01.149

Disruption mitigation seeks to minimize the deleterious effects of an impending disruption by intentionally terminating the plasma discharge in the most benign manner possible. The challenge in disruption mitigation is to meet three mitigation goals simultaneously: reducing localized thermal loading of surfaces, minimizing electromagnetic forces associated with poloidal halo currents I_{halo}, and avoiding relativistic electron (RE) formation in the high electric field of the current decay phase. High-pressure gas-jet injection is a promising technique to achieve these goals [3] and works by essentially triggering radiative dissipation of the available energy ($W = W_{th} + W_{pol}$). Gas injection disruption mitigation has been demonstrated on several tokamaks with a variety of gas species and gas delivery rates [3–7], and in general has compared favorably versus other mitigation methods, in particular reducing or eliminating RE as compared to high-Z impurity pellet injection [3]. An outstanding question is how well the gas-jet mitigation technique will scale to a device like ITER, and what gas-jet hardware will be necessary? The implementation and modeling of high-pressure gas injection (HPGI) on several present tokamaks will help illuminate design and physics issues for ITER.

The Alcator C-Mod tokamak [8] offers unique opportunities to study the extrapolation of HPGI to ITER. C-Mod is a compact ($R = 0.67$ m) tokamak with a high toroidal magnetic field ($B_T > 5.4\ \mathrm{T} = B_{T,ITER}$), allowing it to access relatively unique plasma regions among present devices. C-Mod has similar plasma shape and divertor topology as ITER, albeit at a smaller scale ($R_{ITER} = 6.2\ \mathrm{m} \sim 10 \times R_{C\text{-}Mod}$). C-Mod can achieve central pressure $p \sim 5$ atm [9] at $B = 5.4$ T, essentially matching the ITER kinetic and total magnetic pressures, providing critical insight to the complex dynamics of impurity penetration [10–12]. The large poloidal field of C-Mod results in large $W_{pol} \sim B_p^2$ stored in a small volume. C-Mod therefore has a high volumetric energy density in comparison to other present tokamaks, $w \sim (W_{th} + W_{pol})/V_{plasma} \sim 0.8\ \mathrm{MJ\ m^{-3}}$, closely matching ITER ($w \sim 1.2\ \mathrm{MJ\ m^{-3}}$, $W_{th}/W \sim 0.3$). Note that mitigation must dissipate this energy by radiation on the intrinsic disruption timescale of the device. The small size of C-Mod results in fast disruption timescales: both $n = 0$ vertical motion of the plasma during vertical displacement event (VDE) disruptions and the dissipation of W_{pol} during the current quench (CQ), occur in $\tau \sim 1$ ms [13]. Such short timescales pose a challenge to mitigation techniques in terms of the required response time and radiative power density. For example, the rapid CQ of C-Mod, ($L/R_{ITER} \sim 30 \times L/R_{c\text{-}Mod}$), results in a global wall surface transient heating figure of merit ($\sim W/A_{wall}/\tau^{1/2}$) which approaches ITER within a factor of two, despite the 10× higher areal energy density of ITER. Also, the C-Mod current density, $j \sim B/R$, is ~10× larger than other present devices and ITER, providing ideal scaling tests for halo current [14] and CQ equilibrium [15] models. Finally, the C-Mod wall is clad solely in a high-Z refractory metal (molybdenum) with frequent applications of boron films [9]. This 'all-metal' environment serves both as a proxy for the mostly metallic wall (tungsten and beryllium) of ITER, and to compare to the favorable results on wall response with HPGI on the all-carbon DIII-D [16]. For example, the gas diffusion and solubility properties of Mo are very different from carbon, and thus one is obliged to experimentally test the compatibility of large gas injection with a metal wall in a tokamak.

2. Experimental setup on Alcator C-Mod

Alcator C-Mod experiments were carried out on lower single-null diverted discharges with plasma current $I_p = 1$ MA, magnetic field $B_t = 5.2$ T, plasma volume $V \sim 1\ \mathrm{m^3}$ line-averaged density ~2–3 × $10^{20}\ \mathrm{m^{-3}}$, central pressure ~0.2–0.3 MPa, ion-cyclotron heating $P_{ICRH} \sim 2$–3 MW, and stored energies $W_{th} \sim 0.13$ MJ, $W_{pol} \sim 0.6$ MJ.

The gas-jet system consists of a 0.3 l high-pressure (7 MPa) plenum filled with a pure noble gas: helium, neon, argon or krypton. A fast-acting magnetic valve [17] outside the field coils releases gas from the plenum into a constant diameter ($D = 9.2$ mm), delivery tube $L \sim 2$ m in length. The valve is typically opened for ~2 ms, resulting in $N \sim 10^{23}$ gas atoms delivered to the torus, ~300 times the plasma particle inventory. The tube exit 'nozzle' is positioned on the edge of an existing limiter and is ~25 mm distance the plasma edge, maximizing local gas pressure (~0.03 MPa) while avoiding damage to the tube. Further details can be found in [18]. All gas-jet results reported were planned pre-emptive terminations of stable plasmas, although control-system gas-jet triggering capabilities are now available.

3. Experimental results on disruption mitigation

High-pressure noble gas injection causes a rapid, radiative termination of the Alcator C-Mod plasma,

resulting in successful disruption mitigation. An example argon gas-jet termination is compared to an un-mitigated disruption in Fig. 1. The evolution of their plasma equilibriums is shown in Fig. 2. The un-mitigated disruption was caused by an intrinsic impurity burst into the plasma. In the pre-emptive termination, the valve opens at time t_{valve}, building gas pressure at the delivery tube inlet and starting the flow of argon down the pipe (Section 4). Approximately 2.5 ms later, the first signs of edge plasma cooling by the argon are detected from a decrease in the edge soft X-ray emission (not shown). After another 1.5 ms, at $t_{CQ,0}$, central soft-ray emission shows the final thermal quench (TQ) and the current quench begins. The two cases have dramatically different CQ evolutions. In the un-mitigated case, the core plasma becomes vertically unstable and moves down to eventually limit on the top of the outer divertor baffle, resulting in a large poloidal halo current at the loss of closed flux surfaces. In contrast, the argon gas-jet triggers a much faster CQ decay. The core plasma remains relatively well-centered in the vessel and is diverted until close flux surfaces are lost, resulting in substantially lower I_{halo}. No significant runaway electron current was detected in any of the gas-jet mitigation cases. Imaging diagnosed shallow penetration ($r/a > 0.9$) of gas neutrals during the initial phases of gas injection before the current quench,, consistent with recent experiments at DIII-D [10].

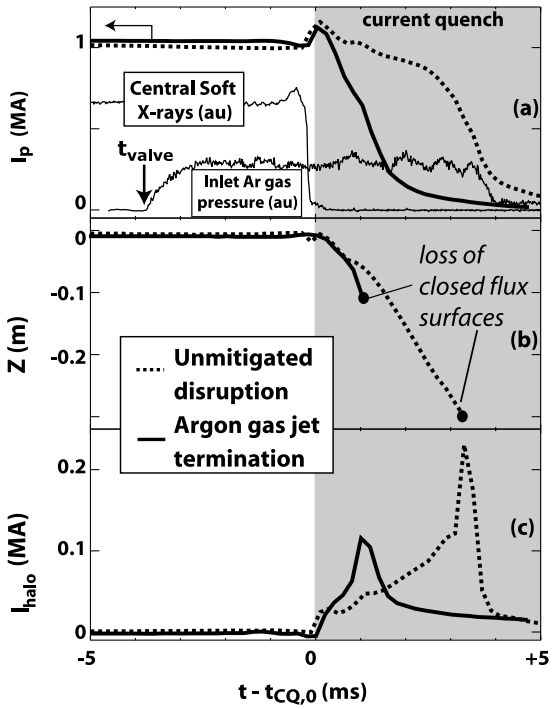

Fig. 1. Evolution of an un-mitigated disruption versus pre-emptive argon gas-jet termination on Alcator C-Mod. (a) Plasma current, I_p. Also shown for the argon case: gas pressure at the delivery tube inlet as the reservoir valve is opened at t_{valve} , central soft X-ray emission showing the rapid thermal quench. (b) Plasma vertical centroid position from equilibrium reconstructions (Fig. 2). (c) Poloidal halo current.

The mitigation results of different gases are summarized in Table 1. Effective halo current mitigation is linked to a larger radiated energy fraction, W_{rad}/W. This is consistent with the idea [19] that higher core plasma radiation rates in the CQ will increase the core plasma resistive decay rate, thus competing against the vertical displacement rate, and reducing the ability of the current channel to move into the wall.

The radiated energy fraction increases with gas atomic number and approaches 85% (Table 1) We believe this approaches optimal radiative dissipation since a fraction of the initial poloidal magnetic energy (field) is outside of the conducting vessel and cannot penetrate through to the plasma volume on a ~2 ms CQ timescale. Higher radiative dissipation (W_{rad}/W) of the high-Z gases is consistent with a significantly decreased surface temperature on the lower divertor surfaces in the cool-down phase after the termination (Table 1). Infrared imaging indicates that the heat load pattern is not toroidally symmetric, but rather concentrated on leading edges, particularly at the top of the outer divertor baffle [18] where the plasma often limits in unmitigated disruptions (Fig. 2).

Increasing plasma density is important in disruption mitigation since radiated power density, $P_{rad} \sim n^2$. Large increases in core plasma line-averaged electron density, $\overline{n_e}$, accompany the C-Mod massive gas injection as seen in Fig. 3. In the early phases of the TQ, only helium increases $\overline{n_e}$, while in the latter TQ phase, >5× increases in $\overline{n_e}$ are found for all gases. The CQ phase sees the highest density, typically pushing $\overline{n_e}$ past the detection limit ~ 3×10^{21} m^{-3} (set by the refraction of the CO_2 laser through the plasma!). The helium cases clearly stand out as having earlier and larger increases in as compared to the higher-Z cases (Ne, Ar, Kr), a result which pertains to particle penetration (examined in Section 5).

The gas-jet terminations are highly reliable and reproducible, and are benign to tokamak operations. Both the timing of the core thermal quench

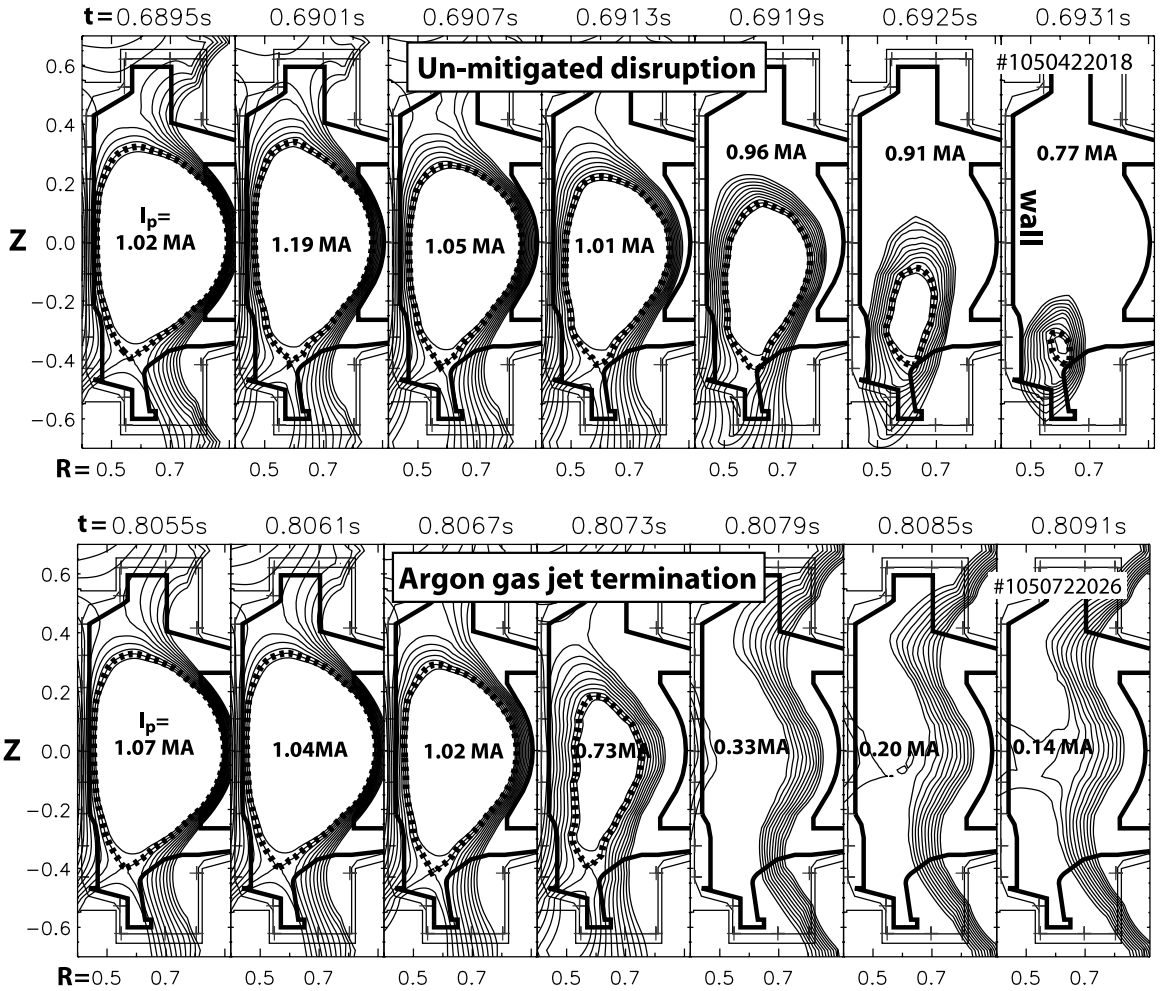

Fig. 2. Evolution of plasma equilibriums reconstructed with a current filament code for an un-mitigated disruption (top) and pre-emptive argon gas-jet termination (bottom). These are the same discharges as shown in Fig. 1.

Table 1
C-Mod gas-jet disruption mitigation with different gases

Gas	W_{rad}/W	$\Delta T_{div.\ baffle}$	I_{halo} (MA)	$(E_{\|}/E_c)_{max}$
None	<0.25	117	198 ± 29	N/A
He	0.36 ± 0.07	77	150 ± 3	3
Ne	0.67 ± 0.08	45	134 ± 9	106
Ar	0.79 ± 0.05	N/A	116 ± 18	154
Kr	0.82 ± 0.07	47	116 ± 13	N/A

W_{rad} is total radiated energy measured by fast bolometry, W is total plasma energy ($W_{th} + W_{pol}$) in target plasma. $\Delta T_{div.\ baffle}$ from IR thermography of a portion of the outer divertor baffle 0.2 s after the termination. $E_{\|}$ is the parallel electric, and E_c is the critical electric field for runaway electron generation.

and the current quench L/R decay rate are well organized to the injected gas species (Fig. 4). The overall response time of the system to trigger a radiative thermal collapse is ~4 ms (Fig. 4(b)), even with the use of the relatively long 2 m delivery tube (see Section 4). The gas injection into the $V \sim 4\ m^3$ vessel results in a post-termination vessel pressure ~40 Pa, and is readily pumped away. No problems are encountered in the breakdown and I_p rampup of the subsequent discharge. This indicates that the injected gas is not significantly implanting into the metal wall so at to deleteriously affect the next discharge by noble gas impurity radiation on its release. As with DIII-D, this is consistent with low sheath potentials at the wall expected from the low plasma temperatures during the gas-jet termination [16]. On C-Mod, un-mitigated disruptions often lead to I_p rampup failure in subsequent discharges (intra-shot wall conditioning, such as glow discharge cleaning, is typically not used on C-Mod). The inference is that this failure is caused by altered

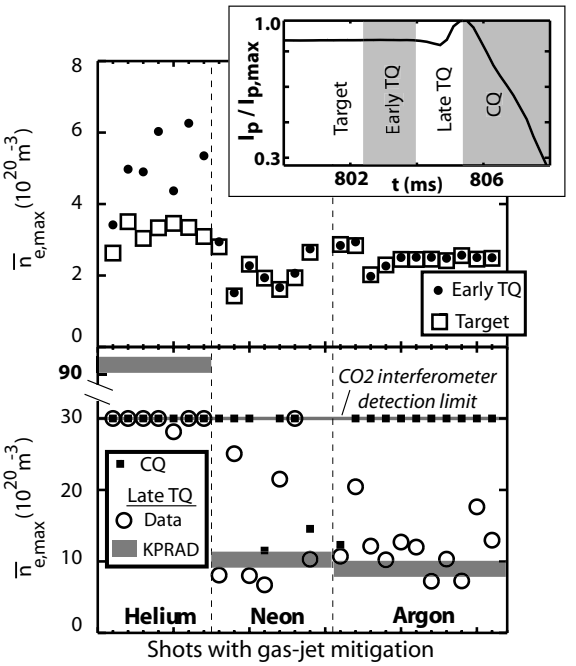

Fig. 3. Evolution of core $\bar{n}_e$ measured with a CO_2 interferometer for different gases. (Inset: definitions of the various phases). The first signs of edge cooling from soft X-rays set the start of the early thermal quench (TQ). The late TQ begins with the first drop in I_p, indicating perturbation of the current profile. Note different vertical scales.

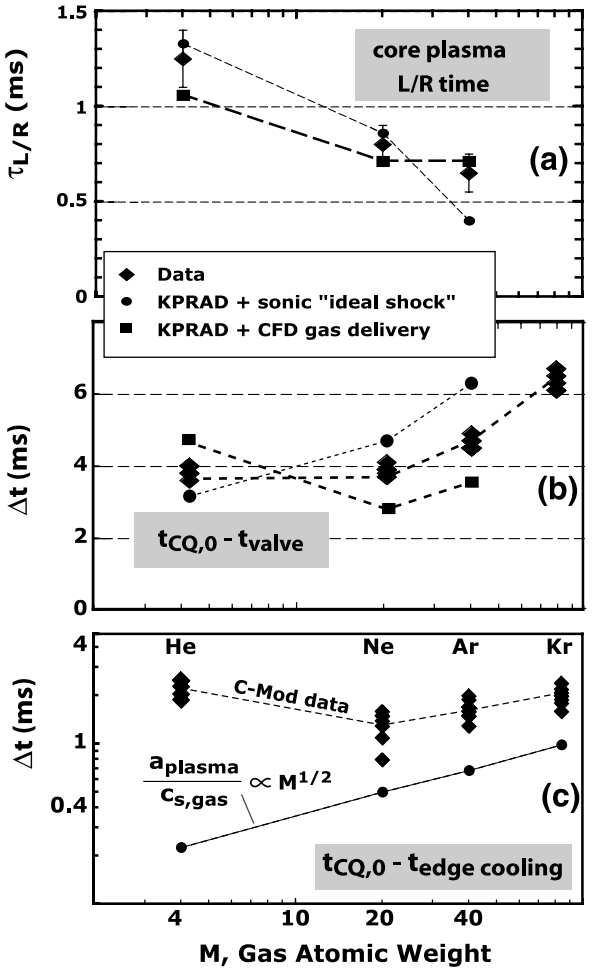

Fig. 4. Predictions of the 0-D (KPRAD) code, using the fitted gas delivery rates (Fig. 5) compared to data. (a) L/R current decay time of core plasma at the start of the CQ. (b) Time delay between the valve opening t_{valve} and $t_{CQ,0}$. (see Fig. 1 for timing definitions.) (c) TQ timescale: time delay between first sign of edge plasma cooling as measured with soft X-rays, $t_{edge\ cooling}$ and $t_{CQ,0}$.

metallic wall fueling or impurity release properties, triggered by the preceding rapid surface temperature excursion during the disruption. The success of I_p rampup in discharges following HPGI is therefore consistent with reduced thermal loading of the plasma-facing Mo walls (Table 1).

4. Gas dynamics and 0-D radiation-energy balance

Knowing the parameters of the gas flow and delivery from the high-pressure reservoir, through the pipes and into the torus/plasma is a basic requirement for understanding gas-jet mitigation. A particular concern is the delivery of gas through a small aspect ratio ($D/L \ll 1$) tube, since it will be easiest to position the gas reservoir and valve outside of the TF and blanket on ITER, ~3–4 m distance from the plasma. In previous studies (e.g. [16]), a constant gas flow rate and exit pressure was assumed into the plasma, calculated with simple particle conservation using the total gas emptied from the reservoir and the valve open time. The gas delivery was simply delayed after the valve opening by, $\tau = L/c_{s,gas} \sim 2$–6 ms (for $L = 2$ m), where $c_{s,gas}$ is the gas sound speed. Recent bench-top tests of the gas-jet hardware [20] indicate that gas delivery is not so efficient and this affects disruption mitigation. For instance the maximum gas pressure for He gas delivery (down a 2 m delivery pipe as used in C-Mod) is not reached until ~ 8 ms after the valve is opened [20] (Fig. 5). To date attempts to model the measured waveforms of gas pressure using 1-D shock-capturing codes have been unsuccessful. Both analytic solutions without friction, and numerical codes with friction, calculate a rise-time of exit gas pressure that is too rapid, indicating that the problem may require 2-D modeling. For practical purposes we have fit the time

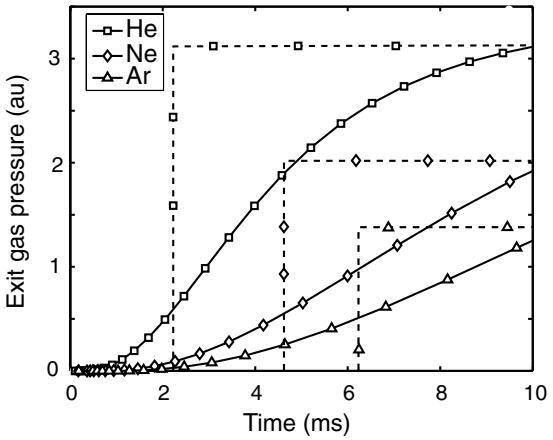

Fig. 5. Gas exit pressure versus time for several noble gases using results from a numerical gas code with an arbitrary fitted friction factor used to match benchtop data [20] (solid lines) for the C-Mod gas-jet hardware parameters (reservoir pressure = 70 atm, pipe length = 2 m, pipe diameter = 9.4 mm). Also shown: gas delivery with a sonic-speed 'idealized-shock' (dashed lines) as used in previous studies [16].

dependence of the experimental data in the 1-D numerical code using an arbitrary, but unrealistic, friction factor, while normalizing the absolute flow rate to the data.

The fit results for gas delivery are summarized in Fig. 5 for the C-Mod gas-jet hardware ($L \sim 2$ m, $D = 9.4$ mm). The calculated local gas pressure at the tube exit follows closely the gas delivery rate, ρv, since the CFD calculated $v_{\rm exit} \sim c_{\rm s,gas}$ is nearly constant. The high-Z gases have slower sound speed $c_{\rm s,gas} \sim M^{1/2}$ and longer delays due to their larger atomic mass, M. The deviation from an ideal shock is more severe for the high-Z gases simply because they spend more time in transit. The early 'dribbling' of high-Z gas (e.g. argon at $\sim$2.5 ms in Fig. 5) is undesirable because $<10^{-3}$ of the total $N_{\rm Ar} \sim 10^{23}$ will begin to trigger a radiative collapse, yet the gas pressure is far from reaching its maximum at 2.5 ms. This problem is particularly acute for C-Mod with its small L/R CQ timescale. The argon gas delivered after the CQ is finished ($t \sim 6$ ms in Fig. 5) is obviously not contributing to the disruption mitigation.

We have used the accurate gas delivery/pressure fits to better constrain the 0-D energy balance calculations of the KPRAD code [15]. KPRAD self-consistently evolves the impurity ionization, impurity radiation, plasma resistivity, ohmic heating and current decay. Such an approach, which treats the impurities in a volume-averaged manner, is necessarily limited since it does not address impurity and MHD dynamics in the thermal quench (Section 5). However, the 0-D calculation has the benefit of having no adjustable parameters and therefore provides a rigorous test of the global energy balance. Anyway, the expectation is that the impurities are well distributed in the core plasma during the CQ due to core stochasticity (e.g. [11]) and the inability of the cold plasma to effectively shield the continued high-pressure gas injection in the CQ (Fig. 1). This result is not inconsistent with the shallow neutral penetration in the TQ.

Comparisons of KPRAD modeling with experimental data are shown in Figs. 3 and 4. KPRAD correctly predicts that maximum $n_{\rm e}$ in the late thermal quench is much larger with He than for the higher-Z gases (Fig. 3), resulting from a combination of the different gas delivery rates (Fig. 5) and the vastly different ionization physics of the impurities. Due to its low-Z, helium tends to cool by dilution, an important aspect of penetration dynamics (Section 5). The core plasma CQ decay times are predicted within experimental uncertainty (Fig. 4(a)), verifying that CQ thermal equilibrium, $n^2 L_{\rm rad} = P_{\rm rad} = \eta j^2$, is primarily set by the atomic physics of the injected impurity, and in particular the ionization potential of the lowest charge state [3]. Including accurate gas delivery improves the agreement between the model and experiment. This ability to predict and externally set the CQ decay rate is highly desirable with regards to vessel and component design, which must consider both forces from halo currents, as well as eddy current forces that increase with faster CQ rates. The time required to thermally quench the plasma after the valve opens, $t_{\rm CQ0} - t_{\rm valve}$ (Fig. 1) is predicted within $\sim$25% or $\pm$1 ms (Fig. 4(b)). The ideal shock model clearly overestimates the quench timescales required for argon and neon. However, the trend with gas species is still not recreated by the codes. A particular surprise is that the predicted time for He is longer than measured, since the calculation assumes essentially instantaneous particle mixing in the core, and again indicates that helium behavior is different in the TQ.

The 0-D code also calculates that the CQ parallel electric field, $E_{\|}$ exceeds the critical electric field (set by total electron density) for relativistic electron generation and amplification (Table 1) [21]. The expected RE gain in C-Mod is $G \sim 3$–4 (i.e. amplification factor $\sim e^{\rm G}$). However, no significant relativistic electron population is observed in any of the

gas-jet cases (RE were observed on C-Mod with high-Z pellet injection). This is consistent with the suppression of RE with $G \sim 4$–5 on DIII-D [3], and points out that enhanced RE transport in the stochastic CQ is likely lowering the requirement for collisional damping [22].

5. Impurity penetration: Data and MHD numerical simulation

The evolution of core profiles through the TQ (Fig. 6) shows a striking difference between the He and Ar cases, consistent with other data (Figs. 3 and 4). The helium case shows strong particle penetration into the core, as witnessed by the 10× density increase that accompanies the propagating cold front in T_e. However the He-induced cold front moves through the core plasma at a velocity substantially less than $c_{s,gas}$ (Fig. 4(c)), clearly breaking the sound speed scaling previously found on DIII-D [3,10]. Conversely, the argon TQ occurs with no change in the central plasma density i.e. without deep Ar particle penetration (as ions or neutrals).

The NIMROD non-ideal MHD code [23] was used to study the dynamics of the gas-jet disruption mitigation by imposing a cooling front at various radial locations near the plasma boundary [11]. It was found that MHD enhanced thermal transport, triggered by $m/n = 2/1$ modes at the $q = 2$ surface, can produce the core thermal quench without a central density increase. Essentially, the central plasma energy is transported to and dissipated by the cold, highly radiating edge where the impurities reside. This initial result, which used $T_{e,0} \sim 4$ keV and low Lundquist number, is shown in Fig. 6 as scaled to our present experiment.

We have now included significant additional physics in NIMROD to address the impurity-plasma dynamics: (1) Impurity ionization, recombination, and radiation using subroutines from the KPRAD code; (2) Neutral penetration using the ablation pressure model at the jet front [24] and (3) Impurities can mix into the core as the plasma density is advected. The initial phase of jet penetration, up to the point of $n \geqslant 1$ MHD onset, has been simulated for both helium and argon (Fig. 6). In

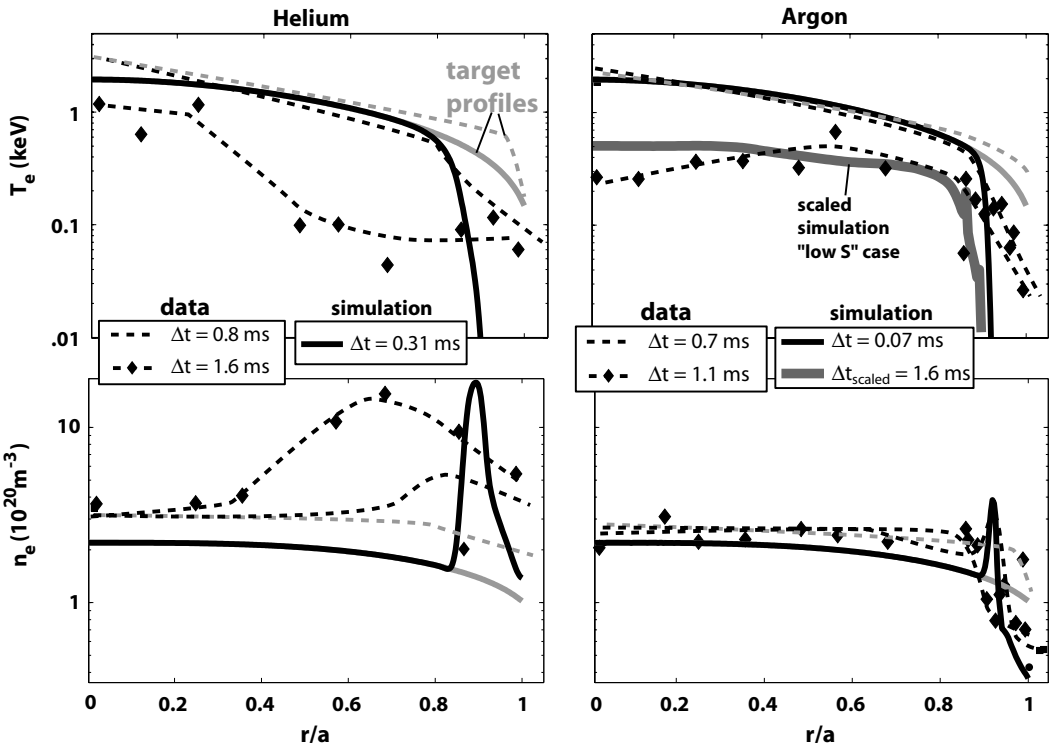

Fig. 6. Plasma profile evolution through the thermal quench. Experimental data (dashed lines) are fits from Thomson scattering with example data points shown. Experimental times, Δt, are relative to first sign of edge cooling measured with soft X-rays. NIMROD MHD simulation (solid lines) times are relative to when impurity neutrals penetrate to the separatrix.

argon simulations, the jet is unimpeded by the jet ablation pressure due to the very rapid cooling of the plasma in the jet vicinity. Thus, the jet propagates inward at the sound speed, triggering $n = 1$ mode growth in under 0.1 ms or ~2 cm of jet penetration, but without significant density increase. Despite a much faster sound speed, the helium jet is significantly impeded by the ablation pressure, and penetrates slower than the argon jet. Dilution cooling is as significant as radiative cooling for He, whereas argon is dominated by radiative cooling. Therefore, helium disturbs the force balance less significantly as the cooling front propagates despite the much large density increase with He. The helium jet triggers an $n = 1$ instability on a slower timescale ~0.25 ms. While preliminary, these results are encouraging that the interplay between the radiation of the impurities and the plasma MHD response can be addressed in the simulations. Simulations that carry through the remainder of the TQ are in progress.

6. Summary of extrapolation to ITER

The experimental results are encouraging for ITER. Gas-jets deliver reliable and substantial disruption mitigation of thermal loads and halo currents at the ITER field and pressure. The gas injection is compatible with a metallic wall. The gas-jets provide sufficient radiative energy dissipation on a timescale even faster than required for ITER. Runaway electrons are suppressed, however a better understanding of this suppression is still required for ITER. Present 0-D calculations of the gas delivery and global plasma response match important experimental data such as overall quench time and the current quench L/R time. However deep gas and/or impurity penetration is not required for mitigation, relieving technical requirements for the gas pressure in ITER. Presently it is not possible to accurately predict the necessary gas pressures (reservoir and at the plasma edge) or particle delivery rate required for ITER since with fixed delivery hardware these cannot be varied independently. Furthermore, it appears that the interactions between the gas and edge plasma are complex but critical to understanding the mitigation, and the controlling parameters of these interactions are not yet identified. Initial studies with NIMROD show that radiation-induced MHD plays a critical role in thermal quench particle and energy dynamics. The future application of a newly available version of NIMROD, with more complete atomic physics, will help increase our confidence in designing efficient disruption mitigation for ITER.

Acknowledgements

This work was supported by the US Department of Energy under the C-Mod Cooperative Agreement #DE-FC02-99ER54512, Contract #DE-AC05-00OR22725, and Grant #DE-FG02-04ER54762. This research used resources of the National Energy Research Scientific Computing Center, which is supported by the Office of Science of the US Department of Energy under Contract No. DE-AC03-76SF00098.

References

[1] ITER Physics Expert Group on Disruptions Plasma Control and MHD, et al., Nucl. Fus. 39 (1999) 2251.
[2] S.C. Jardin et al., Fus. Eng. Design 48 (2000) 281.
[3] D.G. Whyte et al., Phys. Rev. Lett. 89 (2002) 055001.
[4] M. Bakhtiari et al., Nucl. Fus. 45 (2005) 3.
[5] K.H. Finken et al., Nucl. Fus. 41 (2001) 1651.
[6] G. Pautasso et al., Nucl. Fus. 42 (2002) 100.
[7] V. Riccardo, in: 30th European Physical Society Conference on Controlled Fusion and Plasma Physics, 7–11 July 2003 Plasma Physics and Controlled Fusion, St Petersburg, Russia, 45, 2003, p. 269.
[8] I.H. Hutchinson et al., Phys. Plasmas 1 (1994) 1511.
[9] B. Lipschultz et al., Phys. Plasmas 13 (2006) 56117-1-12.
[10] E.M. Hollmann et al., Nucl. Fus. 45 (2005) 1046.
[11] V.A. Izzo, Nucl. Fus. 46 (2006) 541.
[12] V. Rozhansky et al., Nucl. Fus. 46 (2005) 367.
[13] R.S. Granetz et al., Nucl. Fus. 36 (1996) 545.
[14] D.A. Humphreys et al., Phys. Plasmas 6 (1999) 2742.
[15] D.G. Whyte et al., in: 24th European Conference on Controlled Fusion and Plasma Physics, Berchestgaden, Germany, 21A, 1137, p. 1997.
[16] D.G. Whyte et al., J. Nucl. Mater. 313–316 (2003) 1239.
[17] S.L. Milora et al., Rev Sci. Instrum. 57 (1986) 2356.
[18] R. Granetz et al., Nucl. Fus. 26 (2006) 1001.
[19] D.G. Whyte et al., Fus. Sci. Technol. 48 (2005) 954.
[20] S.K. Combs et al., in: 20th IEEE/NPSS Symposium on Fusion Engineering, SOFE 03, San Diego, CA USA, 2003, p. 470.
[21] M.N. Rosenbluth et al., Nucl. Fus. 37 (1997) 1355.
[22] R.W. Harvey et al., Phys. Plasmas 7 (2000) 4590.
[23] C.R. Sovinec et al., J. Comput. Phys. 195 (2004) 355.
[24] P.B. Parks et al., Fus. Technol. 35 (3) (1999) 267.